

Results From the Deep Convective Clouds-Based Response Versus Scan-Angle Characterization for the MODIS Reflective Solar Bands

Amit Angal¹, Xiaoxiong Xiong, Qiaozhen Mu, David R. Doelling, Rajendra Bhatt, and Aisheng Wu²

Abstract—The Terra and Aqua Moderate-Resolution Imaging Spectroradiometer (MODIS) scan mirror reflectance is a function of the angle of incidence (AOI) and was characterized prior to launch by the instrument vendor. The relative change of the prelaunch response versus scan angle (RVS) is tracked and linearly scaled on-orbit using observations at two AOIs of 11.2° and 50.2° corresponding to the moon view and solar diffuser, respectively. As the missions continue to operate well beyond their design life of six years, the assumption of linear scaling between the two AOIs is known to be inadequate in accurately characterizing the RVS, particularly at short wavelengths. Consequently, an enhanced approach of supplementing the on-board measurements with response trends from desert pseudoinvariant calibration sites (PICS) was formulated in MODIS Collection 6 (C6). An underlying assumption for the continued effectiveness of this approach is the long-term (multiyear) and short-term (month to month) stability of the PICS. Previous work has shown that the deep convective clouds (DCC) can also be used to monitor the on-orbit RVS performance with less trend uncertainties compared with desert sites. In this paper, the raw sensor response to the DCC is used to characterize the on-orbit RVS on a band and mirror-side basis. These DCC-based RVS results are compared with those of C6 PICS-based RVS, showing an agreement within 2% observed in most cases. The pros and cons of using a DCC-based RVS approach are also discussed in this paper. Although this reaffirms the efficacy of the C6 PICS-based RVS, the DCC-based RVS approach presents itself as an effective alternative for future considerations. Potential applications of this approach to other instruments, such as Suomi National Polar-orbiting Partnership, Joint Polar Satellite Systems, and Visible Infrared Imaging Radiometer Suite, are also discussed.

Index Terms—Calibration, collection 6 (C6), deep convective clouds (DCC), desert, Moderate-Resolution Imaging Spectroradiometer (MODIS), response versus scan angle (RVS).

I. INTRODUCTION

AS BOTH Terra and Aqua Moderate-Resolution Imaging Spectroradiometer (MODIS) instruments continue to

Manuscript received April 23, 2017; revised September 1, 2017; accepted September 30, 2017. Date of publication November 10, 2017; date of current version January 26, 2018. This work was supported by the NASA MODIS and CERES projects. (Corresponding author: Amit Angal.)

A. Angal and Q. Mu are with Science Systems and Applications Inc., Lanham, MD 20706 USA (e-mail: amit.angal@ssaihq.com).

X. Xiong is with Sciences and Exploration Directorate, NASA Goddard Space Flight Center, Greenbelt, MD 20771 USA.

D. R. Doelling is with the NASA Langley Research Center, Hampton, VA 23681 USA.

R. Bhatt is with Science Systems and Applications Inc., Hampton, VA 23666 USA.

A. Wu was with Science Systems and Applications Inc., Lanham, MD 20706 USA. He is now with Sigma Space Corporation, Lanham, MD 20706 USA.

Color versions of one or more of the figures in this paper are available online at <http://ieeexplore.ieee.org>.

Digital Object Identifier 10.1109/TGRS.2017.2759660

operate well beyond their designed life of six years, a sustained calibration effort to maintain the accuracy of the MODIS level 1B (L1B) products becomes more and more important. The 20 reflective solar bands (RSBs) of MODIS, covering the spectral range from 0.41 to 2.1 μm , support numerous land, ocean, and atmospheric studies. Two RSBs are imaged at nadir with a nominal resolution of 250 m, five RSBs at 500 m, and the remaining at 1 km. MODIS employs a two-sided scan mirror continuously rotating at 20.3 r/min. The reflectivity of each side of the scan mirror is a function of the angle of incidence (AOI), which needs to be accounted for in the calibration algorithm. As the MODIS scan mirror rotates, each side scans its on-board calibrators as well as the earth-view (EV) port. The RSBs are calibrated primarily using the solar diffuser (SD) observations, with its on-orbit degradation tracked using an SD stability monitor (SDSM). Additional inputs from lunar measurements and response trends from the pseudoinvariant desert sites are necessary to track the sensor's response versus scan angle (RVS). For the RSBs, the specified uncertainty at the typical scene level is 2% in reflectance and 5% in radiance. More details on the MODIS instruments, the RSB calibration algorithms, and on-orbit performance can be found in [1]–[3].

As the instruments continue to age, the single largest challenge for the MODIS RSB is a sustained accuracy in the on-orbit RVS characterization. The RSB RVS was characterized prior to launch by the instrument vendor for both instruments [4], [5]. Prior to MODIS C6, the on-orbit RVS, relative to the prelaunch value, was characterized using a combination of on-orbit solar and lunar gains, acquired at two different AOIs of 11.2° and 50.2° [6]. At the time of this writing, the majority of RSBs on each MODIS instrument continue to meet the calibration requirements by using the RVS approach that relies only on the on-board calibrators [7]. However, the large degradation in the short-wavelength RSB coupled with other instrument issues led to a necessity in the modification of the on-orbit RVS characterization algorithm after about five years on-orbit. For these short-wavelength bands, the RVS is derived by supplementing the on-orbit gain with response trends from pseudoinvariant desert sites to accurately describe the scan-angle-dependent behavior. This approach is implemented for MODIS C6.

Although the current RVS approach continues to perform satisfactorily, the consideration of alternative operational approaches and further improvements need to be explored and evaluated considering the stringent requirements and wide-scale applications of the MODIS L1B products. One such

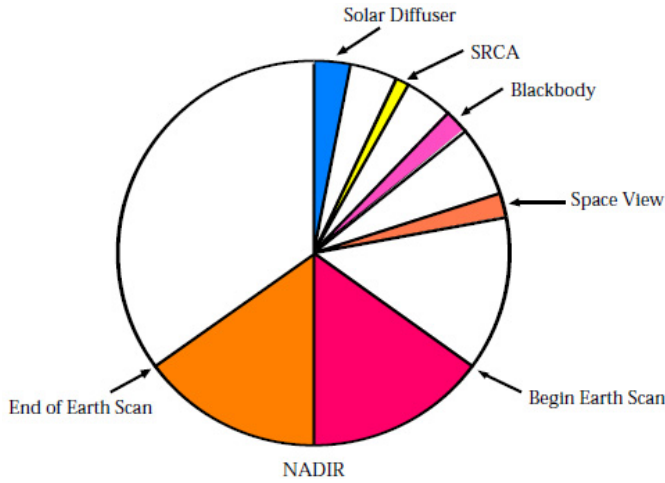


Fig. 1. MODIS scan viewing sequence of the on-board and EV.

approach, the focus of this paper, is using the deep convective clouds (DCC) to track the scan-angle dependence of MODIS RSB on-orbit. Extensive work has been done by Doelling *et al.* [8] to characterize the DCC as invariant calibration targets to facilitate the calibration in the reflective solar region. The DCC are near-isotropic solar reflectors primarily found in the tropics. DCC are bright targets, therefore having a high signal-to-noise ratio, and are located at the tropopause, where the radiative impact of the atmospheric water vapor absorption and aerosols is minimal. Furthermore, DCC exhibit a near-flat spectral response for wavelengths less than $1 \mu\text{m}$ and can be easily identified using a simple infrared (IR) threshold as they are cold targets in the relatively warm tropical regions. A literature review of the previous work and the motivation for this paper are elucidated in Section II. Sections III and IV describe the methodology and the results obtained from this approach. Potential applications of this DCC-based RVS characterization to other sensors, such as to the Visible IR Imaging Radiometer Suite (VIIRS) on Suomi National Polar-orbiting Partnership (SNPP) and future Joint Polar Satellite Systems (JPSS) missions, are also discussed.

II. MOTIVATION

A. Description of RVS Estimation

The MODIS RSB L1B primary data product is the EV top of the atmosphere (TOA) reflectance factor, $\rho_{\text{EV}} \cdot \cos(\theta_{\text{EV}})$, determined by the following expression:

$$\rho_{\text{EV}} \cdot \cos(\theta_{\text{EV}}) = (m_1/\text{RVS}) \cdot dn_{\text{EV}}^* \cdot (d_{\text{ES, EV}})^2 \quad (1)$$

where θ_{EV} is the solar zenith angle of the EV pixel, m_1 is the calibration coefficient derived from SD observations, RVS is the response versus scan angle, and dn_{EV}^* is the EV digital number with corrections applied for the background and instrumental temperature effects. The $d_{\text{ES, EV}}$ is the earth–sun distance (in AU) at the time of the EV observation. The ratio of m_1/RVS denotes the gain of the instrument at any given

TABLE I
FRAME NUMBER TO AOI CONVERSION

Sector	SD	SRCA	BB	SV	EV
Frames	50	15	50	50	1- 1354
AOI	50.25	38.25	26.8	11.2	10.5-65.5

frame [3]. The two-sided scan mirror scans the EV and the on-board calibrators, the SD, the spectroradiometric calibration assembly, the blackbody, and the space view, every 1.748 s. The AOI from each of these sources ranges from 10.5° to 65.5° that corresponds to 1354 frames with the relationship shown in (2), where F is the zero-based frame number

$$\theta = \frac{65.5^\circ - 100.5^\circ}{1353} F + 10.5^\circ. \quad (2)$$

Fig. 1 shows the order of scan mirror viewing, while Table I summarizes the number of frames for each view and the corresponding AOI information. For ease of understanding, the frame numbers [1–1354] are used in this paper to represent the various parts of the MODIS swath.

The prelaunch RVS measurements for both MODIS instruments were performed using an SIS-100 to illuminate the scan mirror at multiple AOIs. Using this, a quadratic RVS approximation as a function of frame was formulated [5]. The on-orbit RVS, normalized to the prelaunch value RVS, was characterized using the responses from the SD at frame 978 and the moon at frame 17. This approach continues to work reasonably well for a majority of the RSB of both instruments after several years on-orbit and is still employed to track the on-orbit RVS for Terra MODIS bands 11–19 and Aqua MODIS bands 10–19. The short-wave IR (SWIR) bands 5–7 and 26 have performed satisfactorily using the prelaunch RVS. In the case of the remaining short-wavelength bands, the linear interpolation using the SD and lunar RVS changes showed a deficiency in accurately describing the AOI dependence, resulting in long-term drifts in the calibrated measurements and various science products. When the L1B Collection 6 (C6) began, the MODIS Characterization Support Team (MCST) implemented an enhanced approach for the on-orbit RVS characterization of these bands. The approach supplemented the on-board gains with the long-term response trends from the pseudoinvariant desert sites (PICS) (Libya 1, Libya 2, and Libya 4) to achieve a more accurate AOI dependence. This approach, referred to as the EV-based RVS approach, has mitigated the long-term drifts observed from the on-board-based RVS and, as a result, improved the calibration quality of the L1B and various downstream products. Similar improvements in the C6 have been reported by Levy *et al.* [9], Lyapustin *et al.* [10], and others. In Collection 5 (C5), only the responses (gains) from on-board SD and lunar observations are used to characterize the on-orbit RVS. A detailed description of the various RVS algorithms and the impact on the long-term reflectance trends can be found in [7].

An example of the impact of the MODIS Collection 5 (C5) forward processing calibration adjustments on the science product is evident from the Clouds and Earth's Radiant Energy

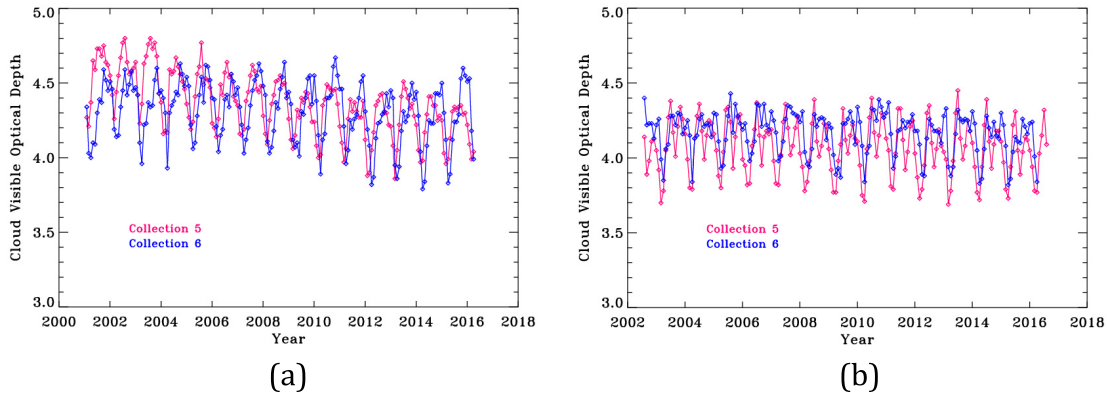


Fig. 2. Optical depth plots for (a) Terra and (b) Aqua MODIS derived using C5 (pink curve) and C6 (blue curve).

System (CERES) cloud property retrievals performed using Terra and Aqua MODIS data. The CERES project does not use the official cloud properties derived by the MODIS Atmospheric Science Team, but retrieves cloud properties using entirely different algorithms specifically designed to aid in the conversion of CERES observed radiances into fluxes [11]. The log of the cloud optical depth is approximately proportional to the MODIS band 1 ($0.65 \mu\text{m}$) radiance. Terra MODIS experienced an SD door malfunction in May 2003 and the door remained in the open position since then. This has accelerated rate of SD degradation due to more exposure resulting in a sharp transition between the two epochs (before and after the SD door anomaly) [12]. Fig. 2(a) and (b) shows the optical depth plots for Terra and Aqua MODIS derived using C5 (pink curve) and C6 (blue curve). Prior to 2009, the SDSM degradation was improperly accounted for, and during the first few months of 2009, the SD calibration was adjusted by 1.5% to account for this change in C5 [13]. The impact of this change is lesser at other scan angles, and hence is not observed in the trends shown in Fig. 2(a) and (b). The C5 data are from the CERES SSF1deg-month Ed3A product, whereas the C6 data are from the SSF1deg-month Ed4A product. These two Terra MODIS calibration anomalies can easily be identified in Fig. 2(a). These Terra MODIS C5 calibration anomalies were removed during C6 processing. Aqua MODIS B1 C6 forward processing suggests an RVS trend difference of 1% based on both DCC and desert targets [18], which could result in a cloud optical depth RVS dependence.

B. Introducing DCC in MODIS RVS Estimation

It should be noted that the C6 desert-based RVS approach relies on the underlying assumption that the PICS exhibit excellent temporal stability. Helder *et al.* [14] have recently worked on characterizing the long-term stability of the North African desert sites. Their recent study shows that the limited data acquisition (one every 16 days at a given frame for MODIS) and further reduction in the usable scenes due to clouds and other atmospheric effects impacts the ability of the sites to characterize the inflight satellite sensors [14]. Although the current desert-based RVS approach performs reasonably

TABLE II
MAPPING OF BAND NAMES TO CENTER WAVELENGTHS

Band 1	Band 3	Band 4	Band 5	Band 6	Band 7	Band 26
$0.64 \mu\text{m}$	$0.46 \mu\text{m}$	$0.55 \mu\text{m}$	$1.24 \mu\text{m}$	$1.64 \mu\text{m}$	$2.1 \mu\text{m}$	$1.375 \mu\text{m}$

well for both MODIS instruments, the consideration of alternative operational approaches for on-orbit RVS characterization needs to be investigated to prepare for the scenario that the desert sites exhibit temporal changes (short term and/or long term) [15].

The tropical DCC, with their invariant characteristics, serve as alternative vicarious targets to track the on-orbit RVS change. Long-term stability monitoring using DCC observations involves constructing a probability distribution function (PDF) using an ensemble of DCC samples within a predefined time interval (monthly). Due to saturation issues, the DCC technique is only applied to bands 1, 3–7, and 26, with their band names mapped with their positions on the spectrum in Table II. Doelling *et al.* [16] and Mu *et al.* [17] showed that the typical number of sample sizes for a given MODIS band during a calendar month is around 1 million pixels. If the DCC pixels are uniformly distributed across the MODIS scan-angle range, DCC observations can be a useful resource to track the on-orbit RVS change. Bhatt *et al.* [18] demonstrated the feasibility of RVS tracking utilizing DCC observations for selecting Aqua MODIS bands utilizing subsampled $2\text{-km} \times 2\text{-km}$ calibrated radiance products designed for the CERES project. This paper performed an assessment (effectiveness) of the Aqua MODIS RVS correction that is derived by MCST using a combination of on-board calibration sources (SD and lunar) supplemented by the desert measurements. The correction factors derived by Bhatt *et al.* [18] are to be applied on top of the L1B calibrated products (for GEO calibration) to account for any RVS inadequacies that may exist.

In this paper, the DCC-based RVS approach is formulated and calculated at the L1A-level at the nominal pixel resolution and instrument-level normalized response for the applicable bands for both MODIS instruments. This allows

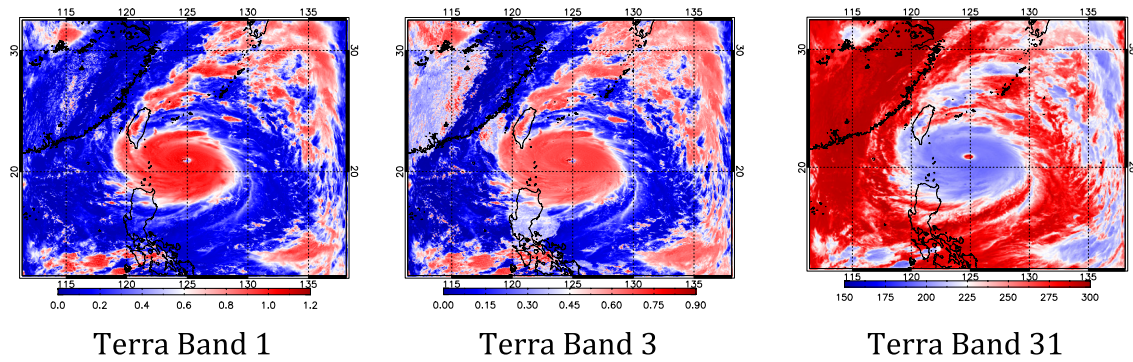


Fig. 3. Terra MODIS granule (2016089.0225) shows TOA reflectance for (Left) band 1 ($0.65 \mu\text{m}$) and (Middle) band 3 ($0.48 \mu\text{m}$) and BT from (Right) band 31 ($11 \mu\text{m}$) for a granule with DCC pixels.

TABLE III
PARAMETER VALUES FOR DCC IDENTIFICATIONS AND DCC REFLECTANCE RETRIEVALS IN THE MODIS DCC TECHNIQUE.
BT11: 11- μm BT; REF: REFLECTANCE

BT Threshold (K)	Uniformity Filter Thresholds		PDF Bin (Ref)	Data Collection Time Interval
	BT11 (K)	Ref (%) Block Size (Pixel \times Pixel)		
205	1	3 3 \times 3	0.001	monthly

for a mirror side and possible detector-separation of the RVS that was not possible with CERES subsampled calibrated radiance data set [18]. In addition, this paper takes advantage of the MODIS channel specific DCC thresholds in [17] not incorporated in [18]. The various thresholds used for this paper are summarized in Table III. Also demonstrated in this paper is the readiness of DCC to serve as an independent target in validation or in an alternative approach to the current desert-based RVS employed in C6. Section III describes the detailed methodology and various data reduction details. The results are discussed in Section IV.

III. METHODOLOGY

A. Classification of DCC at Different AOIs and Mirror Sides

Using DCC to monitor the long-term calibration stability of satellite sensors is a two-step process:

- 1) identifying the DCC target pixels using criteria that include a brightness temperature (BT) threshold;
- 2) constructing PDFs of DCC observations and time series of mode reflectances over the classified DCC pixels.

In the case of MODIS RVS tracking, an additional step to classify these DCC pixels as a function of frame number is also necessary. The DCC algorithm [16] prescribes the use of the tropical domain between 30°N and 30°S with an $11 \mu\text{m}$ BT threshold of 205 K as a prerequisite to identify a DCC pixel. An additional criterion, such as standard deviation thresholds in the uniformity test, is applied before constructing a PDF on a monthly basis. The mode reflectances from the monthly PDFs can be tracked as a function of time to provide an assessment of the sensor's on-orbit calibration stability.

In this paper, the tropical domain is also restricted between 30°N and 30°S ; however, only pixels between 95°W and 175°E are chosen for convenience of data processing. The uncertainties associated with the long-term trending need

to be carefully assessed with the reduced data set. Careful considerations are given to the uniformity of the DCC pixel distribution across the entire frame range to avoid introducing a temporal bias. It should be noted that all the data used in this paper are at 1-km spatial resolution. Fig. 3 shows a Terra MODIS image from 2016089.0225 (year, day of year, hour, min in GMT) over the selected region with a predominant presence of DCC pixels. A reflectance image for Terra MODIS bands 1 and 3 and the BT from the thermal band 31 ($11 \mu\text{m}$) is shown in Fig. 3. The L1B data presented throughout this paper, as well as the data shown in Fig. 3, are processed using the C6 algorithm. The criterion of $\text{BT}_{31} < 205 \text{ K}$ is chosen to perform a first-level classification of DCC pixels. Additional criteria (documented in [17]) are implemented to further screen the DCC pixels. Various details associated with the selection of these thresholds can be found in [19].

Each granule is divided into 13 frame ranges, every 100 frames for the first 12 sets and 154 frames (1201–1354) for the last set. The DCC pixels from each frame range are accrued separately and also separated for the mirror-side index before the PDF is constructed. If a uniform distribution of the DCC pixels over the entire frame range is assumed, the total number of DCC pixels obtained to construct a monthly PDF for each frame bin is about a factor of 12 lower than the PDF constructed using the DCC pixels from all the frames. Fig. 4(a) shows a PDF for Terra MODIS band 1, mirror side 1 between frames 300–399, and was constructed using all the DCC pixels from November 2001. As discussed earlier, the mode reflectance of this PDF is tracked over time to evaluate the long-term stability. Similar PDFs are constructed on a per-band, per-mirror side, and per-frame range basis. Fig. 4(b) shows the total number of DCC-identified pixels as a function of frame for every month of 2001. Fig. 4(b) shows a sufficient number of pixels (more than 10 000) available for each frame bin for different months. It is also important to track the interannual DCC frequency. Fig. 5 shows the total number of pixels plotted for all the months during the four representative years. It can be seen that the total number of pixels from the PDF shows a similar trend across multiple years with a slight curvature at either end of the frame range. The spatial resolution of the MODIS products used in this analysis is 1 km at nadir; however, at either end of the scan, this resolution can be as high as 4 km. Also, 3-D cloud effects on the observed radiance dramatically increase for oblique

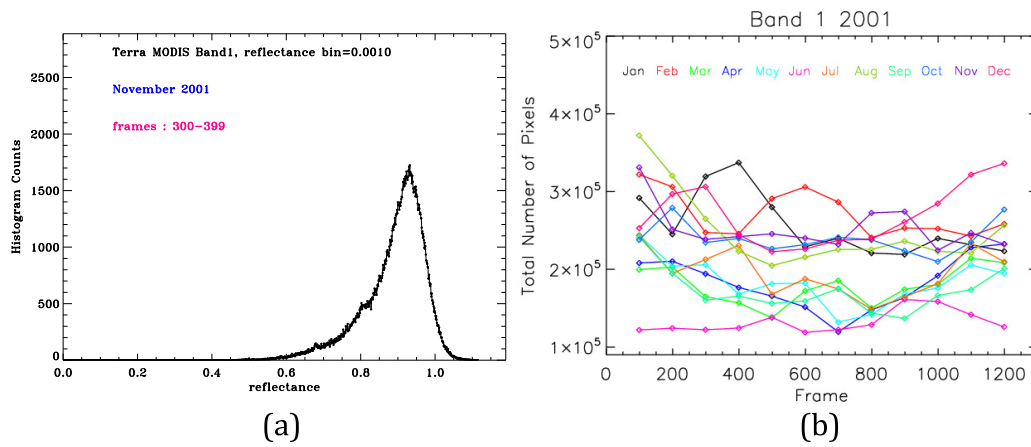


Fig. 4. (a) PDF for Terra MODIS band 1 ($0.65 \mu\text{m}$) from November 2001 DCC pixels. (b) Total number of pixels from each month of 2001 plotted as a function of MODIS frame bins.

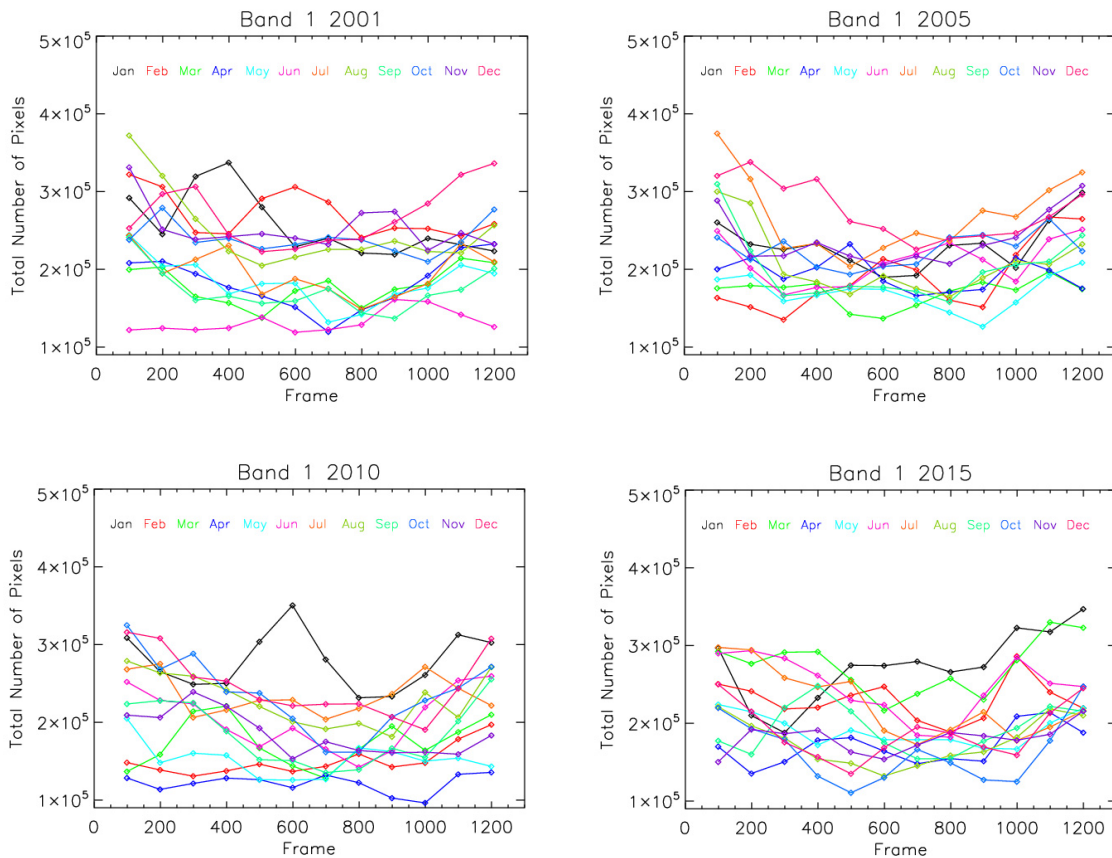


Fig. 5. Total number of pixels per month for Terra MODIS band 1 ($0.65 \mu\text{m}$) from four representative years in the mission.

views, especially for DCC. This is believed to be one of the likely reasons for the increased number of pixels at either edge of the scan. Similar analysis was performed on other bands as well as on the Aqua MODIS bands to ensure a uniform distribution of the DCC pixels used to derive the RVS.

B. Retrieval of the Uncalibrated Responses Over DCC Pixels

As stated earlier, the goal of this paper is to demonstrate the use of DCC to serve as an independent validation or an

alternative approach to the current desert-based RVS employed for the MODIS bands 1, 3, and 4. In other words, the trends from the DCC will be used to derive the on-orbit RVS for these bands. MODIS RSB calibration is reflectance-based with the instrument gain and reflectance factor assuming a linear relationship as described in (1). Due to this linear relationship, the conversion from the calibrated mode reflectance to equivalent uncalibrated quantity is a straightforward process. The mode reflectance derived on a per-monthly basis for every band, frame bin, and mirror side is converted into an equivalent

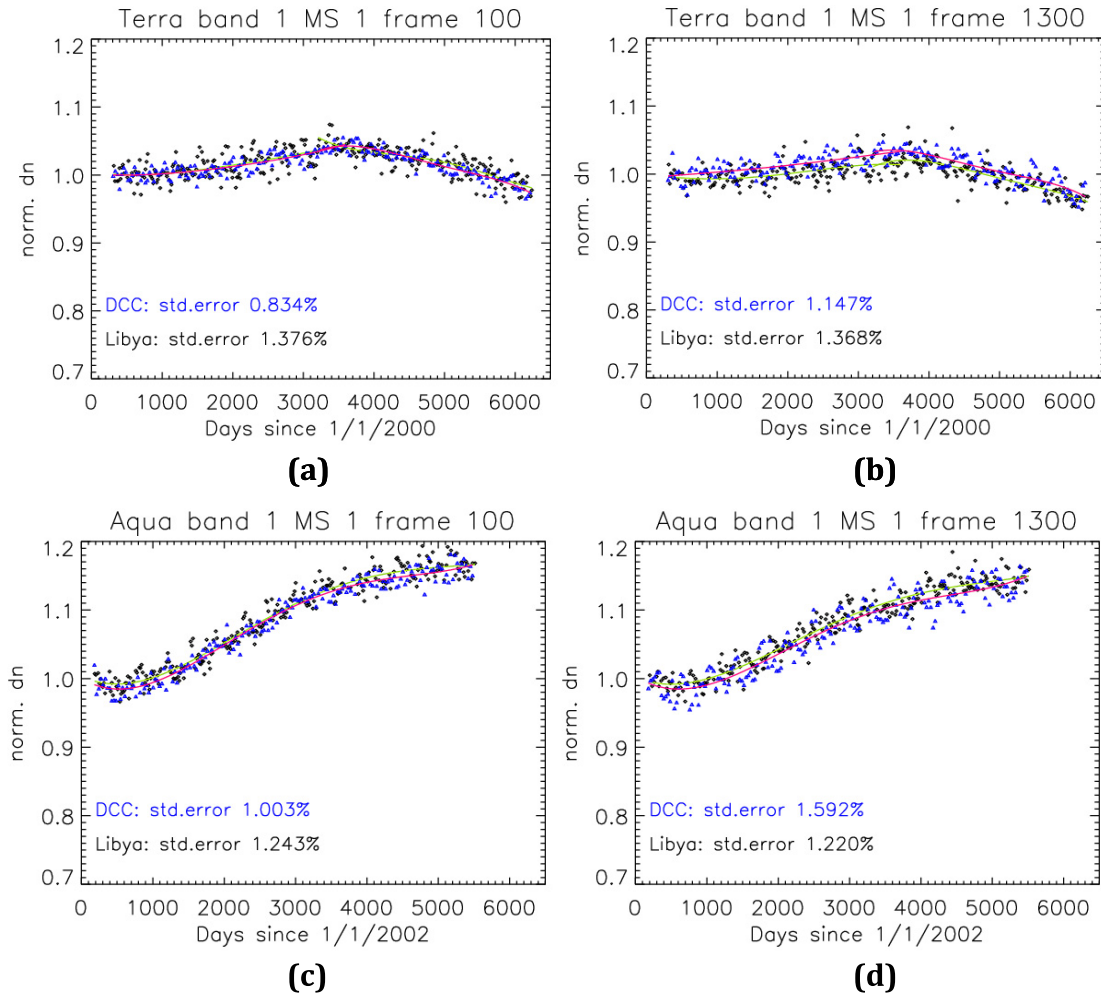


Fig. 6. Normalized response (dn) trending for Terra and Aqua MODIS band 1 ($0.65 \mu\text{m}$), mirror side 1 for a frame at the beginning of the scan (a) and (c) frame 100 and at the end of the scan (b) and (d) frame 1300.

instrument response using the instrument gain (RVS/m_1) and RVS LUT as shown in

$$dn_{EV}^* \cdot (d_{ES_EV})^2 = (RVS/m_1) \cdot \rho_{EV} \cdot \cos(\theta_{EV}). \quad (3)$$

This equivalent instrument response over DCC, along with the on-orbit lunar measurements, is used to derive an alternative version of the RVS, referred to as DCC-based RVS for the remainder of this paper. The detailed algorithm for the desert-RVS characterization has been well documented by Sun *et al.* [7]. The desert-based RVS approach, as implemented in the MODIS C6 L1B, performs a temporal fitting of the on-orbit lunar gain, and the EV response trends obtained at 12 different frame ranges from the North African deserts. In the second step, a fitting along desert site frames is performed and the derived relative response is normalized to the on-orbit lunar gain. The above approach is followed in this paper with the exception that the EV response trends from the desert sites are replaced with those derived from the DCC. Although the formulation of the DCC-based approach follows the C6 implementation, various fitting segments and normalizations are different to adapt to the characteristics of the DCC trends. The results of the response trending from the DCC, its comparison with the desert trends, and

its impact on the derived RVS are discussed in detail in Section IV.

IV. RESULTS AND DISCUSSION

The desert-based RVS approach uses the response trends at 13 different frames (12 in the case of Aqua MODIS) from Libya 1, Libya 2, and Libya 4 sites. The primary reason that multiple sites are chosen is due to the fact that a single site cannot provide sufficient coverage across the entire frame range. For each overpass, a $20\text{-km} \times 20\text{-km}$ region around the site's coordinates is chosen and the average response on a mirror-side level is computed after the necessary corrections (background, earth-sun distance, and so on). It should also be noted that a semiempirical bidirectional reflectance distribution model is also employed to account for the atmospheric and site's dependence on view geometry parameters. Various methodology details can be found in [16] and [20].

A. Temporally Modeling of the DCC-Retrieved Responses and Desert Responses

The normalized response trending from DCC and desert for Terra and Aqua MODIS band 1, mirror side 1 for a frame

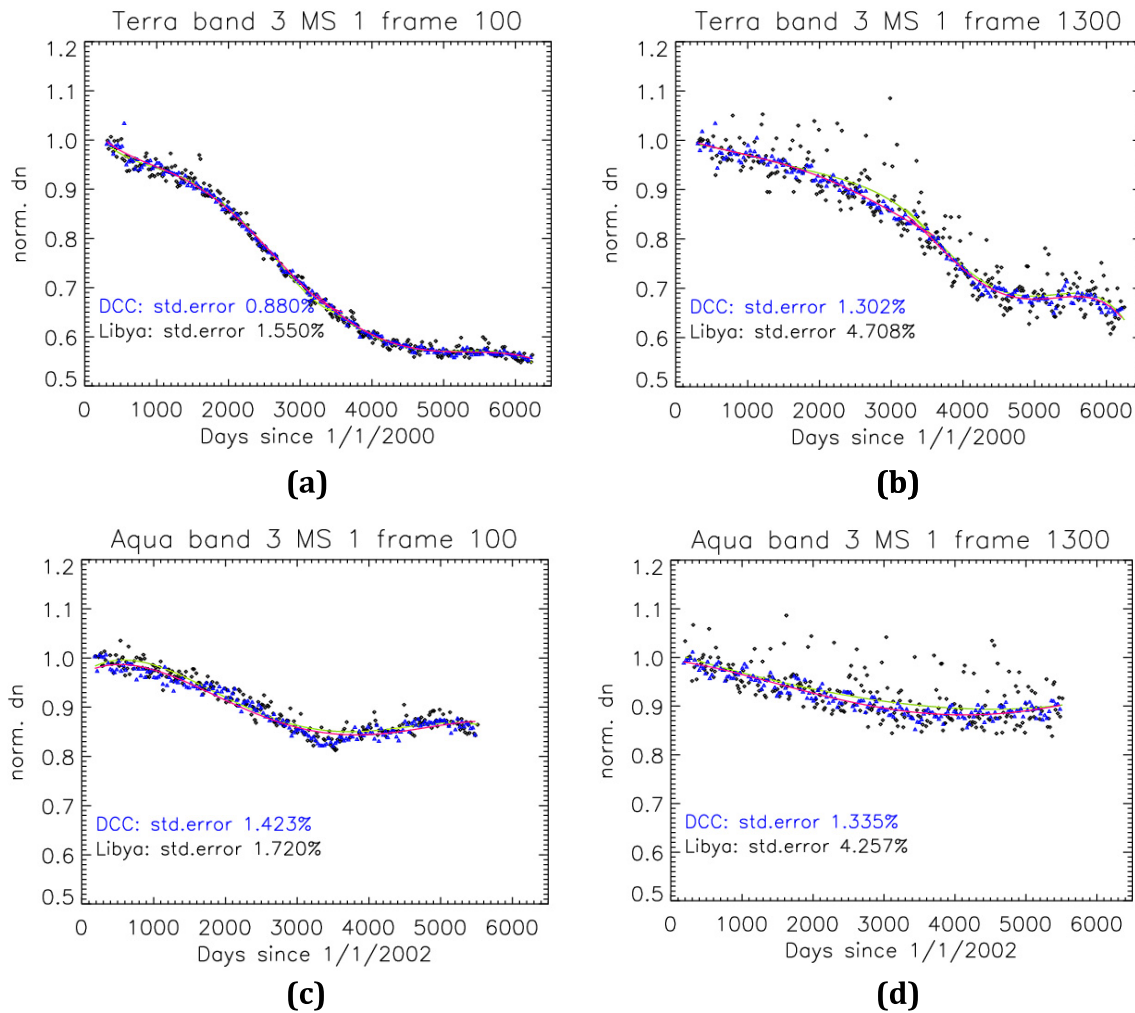


Fig. 7. Normalized response (dn) trending for Terra and Aqua MODIS band 3 ($0.46 \mu\text{m}$), mirror side 1 for a frame at the beginning of the scan (a) and (c) frame 100 and at the end of the scan (b) and (d) frame 1300.

at the beginning of the scan is shown in Fig. 6(a) and (c). Fig. 6 shows the multisegment quadratic model fit to each data set separately, with the normalization point chosen to be the modeled value on the day the nadir door was first opened (day 55 of 2000). In Fig. 6(b) and (d), a similar trend for the end of the scan frame is chosen. The Libyan desert trends are from repeatable observations at particular frames (frame 38 and frame 1329 for Terra MODIS and frame 105 and frame 1313 for Aqua MODIS). The trend from DCC is the equivalent mode reflectance computed using all the DCC pixels from frames 1–100 and frames 1200–1354, respectively. Band 1 ($0.64 \mu\text{m}$) is a near-IR (NIR) band that has experienced less on-orbit RVS changes in comparison with the short-wavelength MODIS bands. This is evident from Fig. 6, where the long-term change observed from the beginning and end of scan time series is within 2% for both instruments. Also, Fig. 6 shows the percentage of the standard error computed relative to the model. In this case, the DCC-based trend is seen to outperform the desert-based trends, yielding lower standard error values. The upward trend (gain increase) observed in band 1 is consistent with the trend shown

by the on-board calibrators (SD and lunar measurements) and indicates that the electronic gain change supersedes the optical gain change for this band.

In comparison with band 1, the short-wavelength band 3 ($0.46 \mu\text{m}$) has experienced significant gain and RVS changes on-orbit, as shown in Fig. 7. The long-term response change at the frame corresponding to the beginning of the scan is seen to be over 40% for Terra MODIS and over 30% for Aqua MODIS. Also noticeable is the large RVS impact, with over 10% differences observed in the long-term response change between the frames corresponding to the beginning and end of the scan for Terra MODIS. In the case of Aqua MODIS, the reversing of the trend is observed around day 3200 [Fig. 7(c)] in the trend from the beginning of the scan. The dip observed in the trends for frame 100 [Fig. 7(c)] is not observed at the end of the scan [Fig. 7(d)] and is indicative of the on-orbit RVS changes. Similar to band 1, the DCC-based trend is seen to outperform the desert-based trend in terms of the standard error. It is noteworthy that the DCC trends at the end of the scan do not exhibit the noisy behavior as observed with the desert trends. The polarization sensitivity of

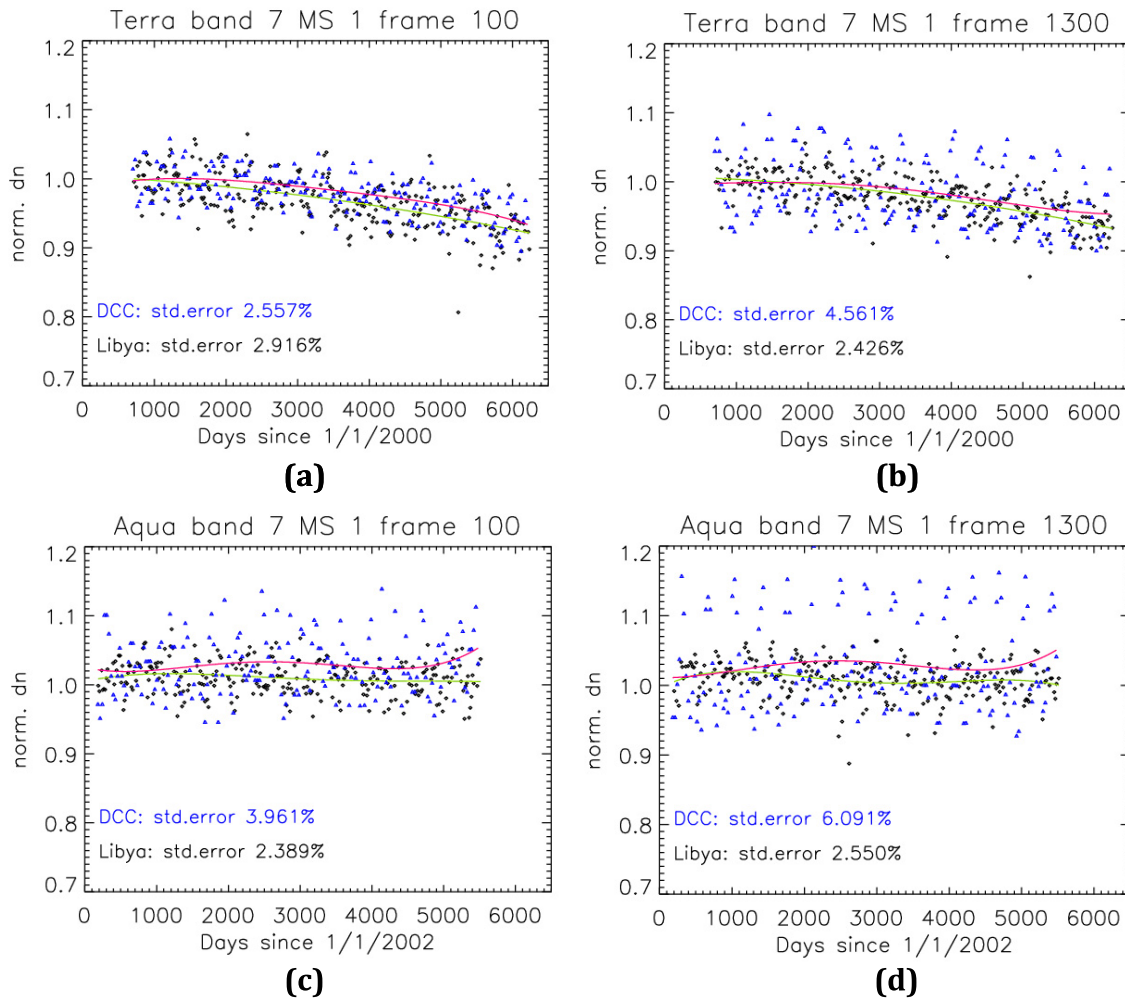


Fig. 8. Normalized response (dn) trending for Terra and Aqua MODIS band 7 ($2.1 \mu\text{m}$), mirror side 1 for a frame at the beginning of the scan (a) and (c) frame 100 and at the end of the scan (b) and (d) frame 1300.

the MODIS instruments, Terra MODIS in particular, has been well documented by Sun and Xiong [21]. Prelaunch characterization revealed the polarization sensitivity for the short-wavelength bands to exhibit mirror-side dependence, with more impact at the end of the scan. Kwiatkowska *et al.* [22] and Meister *et al.* [23] have studied the changes in the MODIS polarization sensitivity on-orbit. The desert surface, viewed through the earth's atmosphere, is partially polarized and manifests itself in the form of fluctuations as observed in the frame 1300 desert trends in Fig. 7. In the case of desert observations, Rayleigh scattering is a dominant source of TOA polarization, which therefore depends strongly on illumination and view geometry. The impacts are maximum during the winter months when the view geometries with scattering angles are near 90° , where the Rayleigh scattering effect is at its maximum. In comparison, the DCC are not impacted by the atmospheric polarization effects, providing a comparatively low-noise trend at the end of the scan. This result reaffirms one of the earlier stated advantages of using the DCC-based approach over the desert-based approach.

The MODIS SWIR bands ($>1.2 \mu\text{m}$) have demonstrated that the prelaunch RVS continues to provide satisfactory

performance for the on-orbit characterization. Nevertheless, a comparison between the desert and DCC trends is presented in Fig. 8 for Terra and Aqua MODIS band 7 ($2.1 \mu\text{m}$). For Terra MODIS, the data from the first few years have been excluded from the plot as it is impacted by several configurations and gain changes in the early mission. As noted by Doelling *et al.* [8] previously, the DCC approach is most suitable for bands with wavelengths less than $1 \mu\text{m}$ as the DCC reflectance is greatly influenced by the cloud particle size for the wavelengths beyond $1 \mu\text{m}$. As shown in Fig. 8, the desert trends seem to outperform the DCC trends in terms of standard errors, and hence are deemed more appropriate to derive a future on-orbit RVS for the MODIS SWIR bands. However, band 26 ($1.375 \mu\text{m}$) is a channel specifically designed to detect cirrus clouds, and as a result cannot provide reliable observations of the desert sites [24]. In this case, the DCC provides a viable alternative to supplement the on-board calibrators for on-orbit RVS characterization. Furthermore, DCC trends at the SD frame can also be used to estimate the unaccounted degradation of the SD on-orbit [25]. The long-term response trends from DCC for band 26 are shown in Fig. 9.

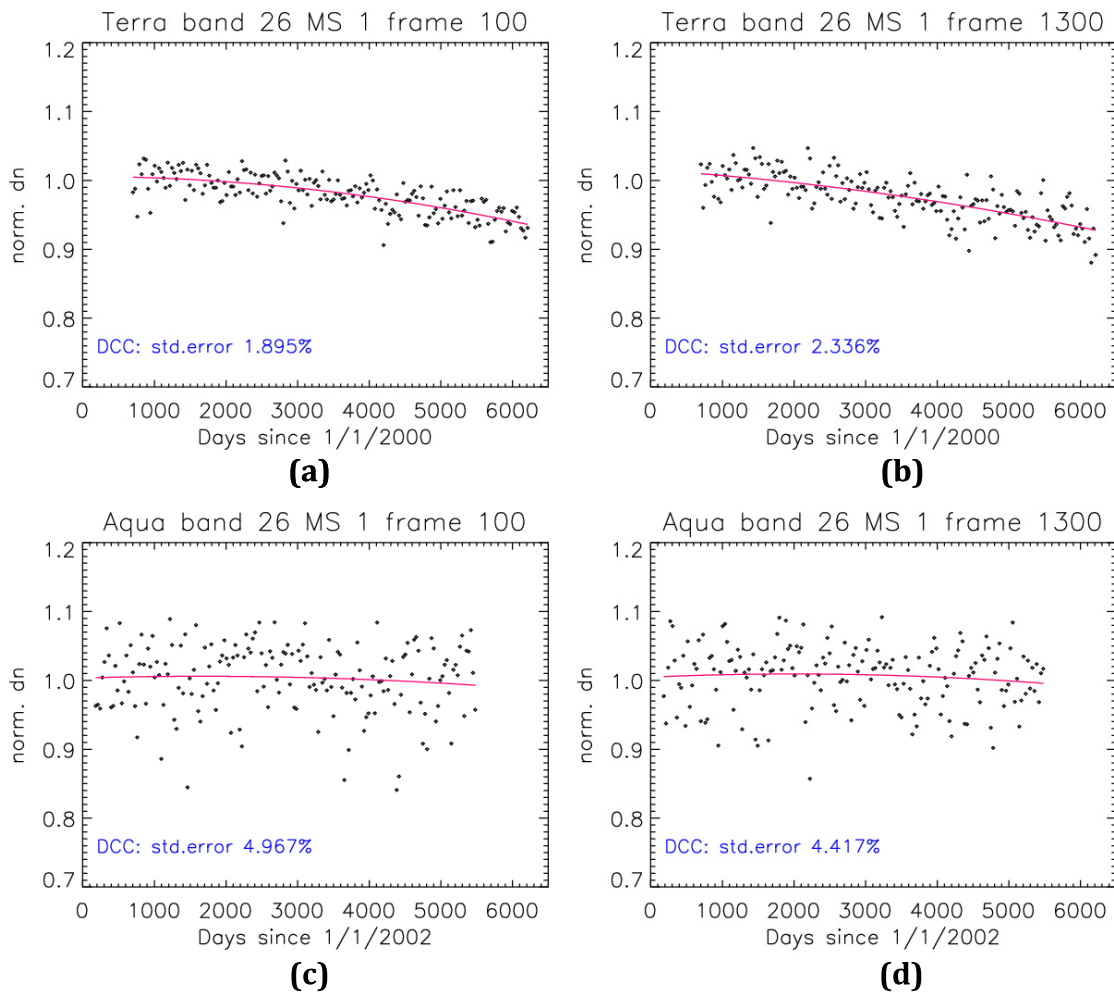


Fig. 9. Normalized response (dn) trending for Terra and Aqua MODIS band 26 ($1.3 \mu\text{m}$), mirror side 1 for a frame at the beginning of the scan (a) and (c) frame 100 and at the end of the scan (b) and (d) frame 1300.

The standard error from DCC and desert responses for other Terra and Aqua MODIS RSB is shown in Figs. 10 and 11, respectively. The percent standard error is plotted for mirror side 1 across the entire frame range for the DCC (blue curve) and desert (black curve). A similar behavior is also observed for mirror side 2. In the VIS/NIR bands (bands 1, 3, and 4), the DCC-based responses perform better than the desert responses, whereas in the SWIR bands (bands 5, 6, and 7), the desert responses are observed to perform better. In the case of band 7 ($2.1 \mu\text{m}$), the standard error from both the sources is observed to be higher than that of the other bands. Fig. 11 shows a similar trend for Aqua MODIS, with a greater standard error for bands 6 and 7 from the DCC trends. The SWIR bands of Aqua MODIS, especially band 6, have known issues of several noisy and inoperable detectors since launch. This results in an inadequately populated PDF and in turn a more noisy behavior. Also, in the case of Aqua MODIS, the standard error from the DCC-based approach is greater than the standard error from the desert-based approach. This behavior is attributed to the necessity of a different bin size as deemed optimal of these bands as discussed by

Mu *et al.* [19]. In this paper, all the bands used the same bin size.

B. Fitting DCC-Retrieved Responses and Desert Responses Over Frames

Using the DCC-retrieved responses as an input, the on-orbit gain (m1 and RVS) for bands 1, 3, and 4 at both the mirror sides of each MODIS instrument is generated over the entire mission. Although this process follows the same RVS characterization methodology as the C6, some modifications in the form of time and frame fitting are performed to accommodate the DCC trends. The temporal trends shown in Figs. 6–9 are used to construct a frame-based relative RVS profile at any given time. The relative RVS curves, normalized to the on-orbit lunar measurement at frame 17, are shown for the two mirror sides of Terra band 3 for four representative years, 2000, 2005, 2010, and 2015. The solid lines denote the trends from the desert data, while the dotted lines denote the DCC-based inputs. The deviation between the beginning and end of the scan is seen to evolve with the mission timeline, with changes of up to 20% in 2015 for mirror side 1. On the

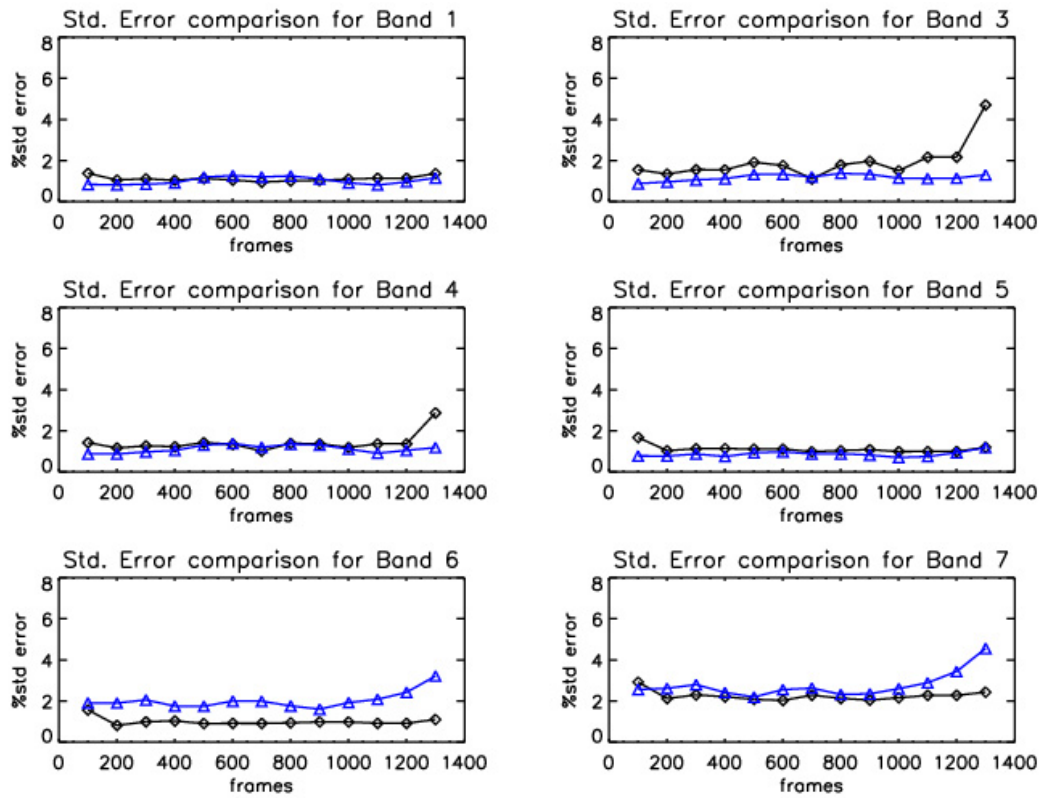


Fig. 10. Comparison of the percent standard error for Terra MODIS bands 1 (0.65 μm), 3 (0.48 μm), 4 (0.55 μm), 5 (1.24 μm), 6 (1.6 μm), and 7 (2.1 μm) using the desert (black curve) and DCC (blue curve) responses.

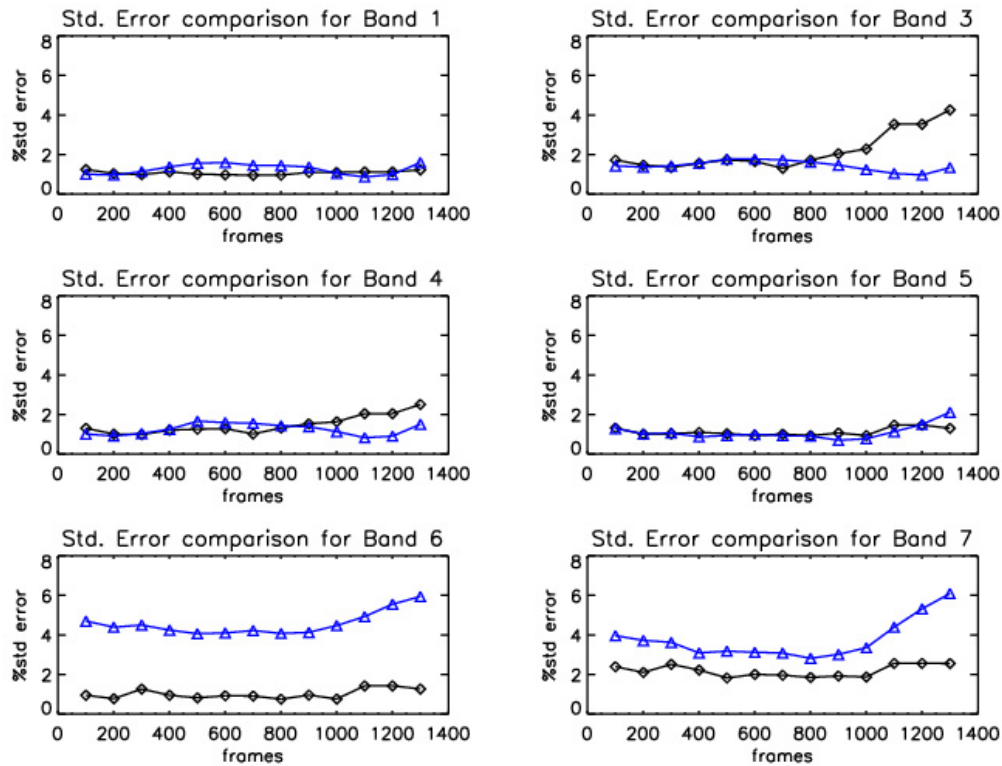


Fig. 11. Comparison of the percent standard error for Aqua MODIS bands using the desert (black curve) and DCC (blue curve) responses.

other hand, the maximum change of about 13% for mirror side 2 is observed in the year 2005. A reasonable agreement is observed between the desert-based and DCC-based relative RVS curves, with more deviation observed at larger frames.

This is an expected result, given the greater noise in the desert trend at large frames as compared to that of the DCC trends. The trends in Fig. 12 further highlight the mirror-side dependence of the RVS.

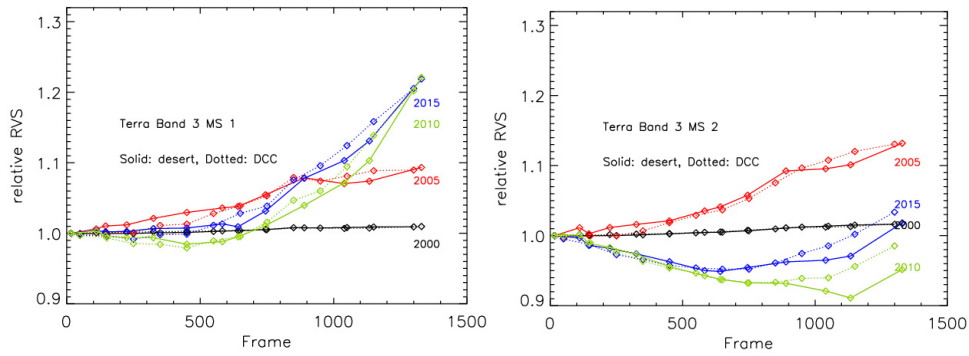


Fig. 12. Relative RVS for Terra band 3 ($0.46 \mu\text{m}$) [(Left) mirror side 1 and (Right) mirror side 2] using desert (C6) and DCC trends.

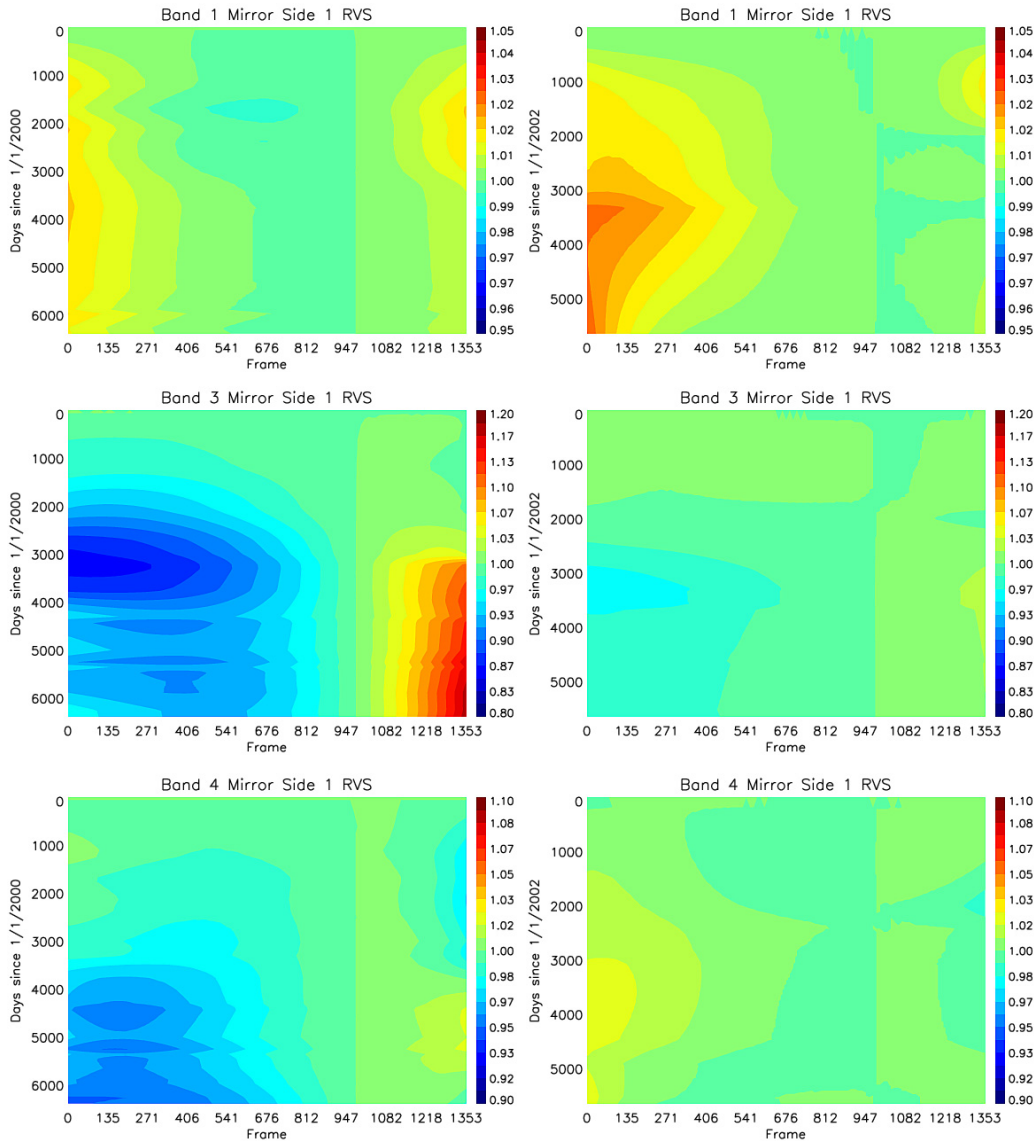


Fig. 13. Surface plot for (Left) Terra and (Right) Aqua MODIS RVS derived using DCC.

Fig. 13 shows a color map of the DCC-based RVS trend for bands 1, 3, and 4 of both MODIS instruments that show the time and AOI dependence. As discussed before, band 3 of Terra MODIS shows most change, both as a function of time and AOI. In comparison with Terra MODIS band 1, the Aqua band 1 shows more change especially at the beginning of the scan.

C. Comparisons of DCC-Based RVS to Desert-Based RVS

The derived gain (m1 and RVS) using the DCC responses is compared with the current C6 gain derived using the desert response trends. A ratio between the C6 gain and the DCC-based gain is plotted as a function of frame for June 1 of three representative years, as shown in Fig. 14. The solid

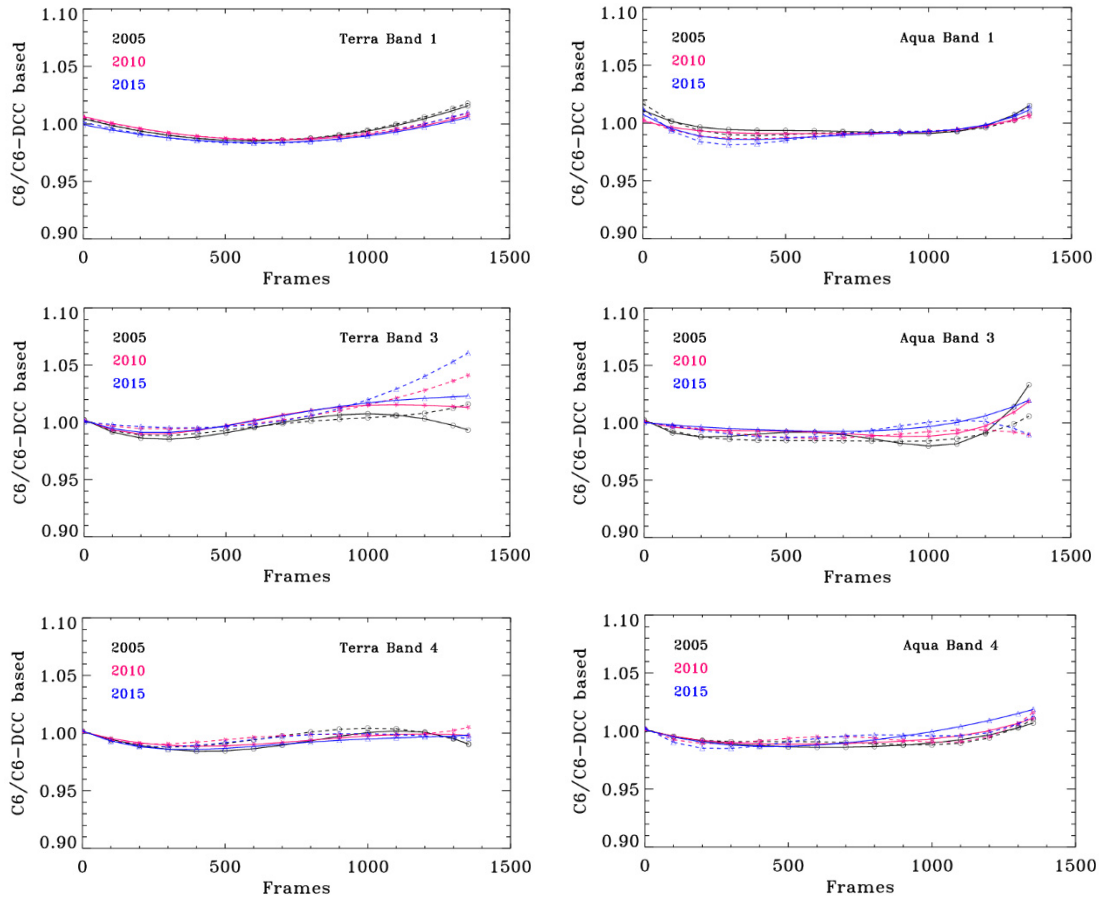


Fig. 14. Agreement between the DCC and desert-based gain (m1/RVS) comparison for MODIS RSB for three representative years for MODIS bands 1 ($0.65 \mu\text{m}$), 3 ($0.48 \mu\text{m}$), and 4 ($0.55 \mu\text{m}$). Solid lines: mirror side 1. Dotted lines: mirror side 2.

lines denote mirror side 1 and the dotted lines denote mirror side 2. As discussed earlier, the time-dependent RVS, based on a combination of on-board and desert trends, is applied to bands 1, 3, and 4 in C6. In the cases of bands 1 and 4, the agreement between the desert- and DCC-based approaches is within 2% for both MODIS instruments. Significant mirror-side differences are observed at the end of the scan, especially for the short-wavelength band 3. The noise in the desert trends due to the atmospheric variations and the absence of those fluctuations in the DCC trends is believed to be the primary reason behind this discrepancy.

The VIIRS instrument onboard the SNPP spacecraft is a scanning radiometer that was designed with a strong MODIS heritage [26]. The lessons learned from the prelaunch and on-orbit calibration of the MODIS instruments have been successfully used in the VIIRS instrument characterization. Similar to MODIS, the VIIRS RSB RVS was also characterized prior to launch and exhibited the wavelength dependence similar to MODIS. Due to the improved design of the VIIRS instrument, it is expected that the on-orbit RVS change in VIIRS is more stable than that in MODIS, exhibiting less changes. This is further reaffirmed by monitoring the long-term trending of the VIIRS RSB over the pseudoinvariant desert sites [27]. The DCC can also be used as an effective alternative to track

the VIIRS RSB RVS performance on-orbit. In addition to all the advantages over the desert-based RVS approach, the DCC-based approach has a wider scope of application in the case of VIIRS due to its dual gain bands that prevent saturation. The technique developed in this paper is also applicable to the future JPSS family of VIIRS instruments.

V. CONCLUSION

The MODIS instruments, with their wide swath, extensive spectral coverage ($0.4\text{--}14.2 \mu\text{m}$), and short repeat cycle (1–2 days), facilitate extensive studies of the earth's land, oceans, and atmosphere. Both MODIS missions continue to operate nearly a decade beyond their design life of six years. The instruments' degradation, particularly at the short wavelengths, has posed significant challenges to maintain the accuracy of the on-orbit RVS characterization, and hence the calibrated L1B products. C6 RVS, based on desert trends supplementing the on-board calibrators, provides a significant enhancement over its predecessor C5, which relied solely on the on-orbit SD and lunar measurements. Although the C6 desert-based approach continues to be able to track the on-orbit RVS changes, the consideration of other operational approaches is warranted for future instrument calibration

support. One such approach, using the DCC-based response trends to derive the instrument-level RVS, is presented in this paper.

The DCC-based RVS approach tracks the time series of instrument responses converted from the monthly reflectance obtained from the PDFs over the identified DCC pixels on a mirror side, frame, and band basis. The long-term DCC responses, along with the on-board lunar measurements, are used to derive the entire mission RVS for bands 1, 3, and 4 (band 2 impacted by saturation). The comparison results to the desert RVS approach used in the current C6 calibrations show good agreements for the RSB presented in this paper. The SWIR bands have experienced a little degradation on-orbit and the prelaunch RVS continues to provide satisfactory performance. Results indicate an agreement of within 2% difference for both the mirror sides of bands 1 and 4 between DCC-based and desert-based gains (m1/RVS). In the case of band 3, up to 5% differences are observed at the larger frames (end of the scan) for mirror side 2. The short-wavelength bands, including band 3, have a known issue of changing polarization sensitivity on-orbit that has more impact at the end of the scan. Unlike the desert responses impacted primarily due to atmospheric absorption and Rayleigh scattering polarization effects, the DCC responses are not impacted by these atmospheric variations. Also, desert sites are more susceptible to temporal short-term and long-term surface reflectance variations. Due to the high signal level, many MODIS bands, especially the high-gain ocean bands, saturate while viewing the DCC. This limits the applications of DCC to track their on-orbit RVS. Despite the limited application scope of the DCC-based RVS approach, it provides a viable alternative to the current desert-based RVS approach in the scenario that the desert sites demonstrate temporal changes. Furthermore, the DCC-based RVS will be used as an independent validation for future reprocessing efforts.

ACKNOWLEDGMENT

The authors would like to thank Dr. X. Geng for the efforts and help in processing the Libyan desert trends. They would also like to thank E. Aldoretta for a technical review of this paper, and previous and current members of the MCST for their work.

REFERENCES

- [1] W. Barnes and V. Salomonson, "MODIS: A global image spectroradiometer for the Earth Observing System," *Crit. Rev. Opt. Sci. Technol.*, vol. CR47, pp. 285–307, 1993.
- [2] X. Xiong *et al.*, "Multiyear on-orbit calibration and performance of Terra MODIS reflective solar bands," *IEEE Trans. Geosci. Remote Sens.*, vol. 45, no. 4, pp. 879–889, Apr. 2007.
- [3] X. Xiong, J. Sun, X. Xie, W. L. Barnes, and V. V. Salomonson, "On-orbit calibration and performance of Aqua MODIS reflective solar bands," *IEEE Trans. Geosci. Remote Sens.*, vol. 48, no. 1, pp. 535–546, Jan. 2010.
- [4] W. L. Barnes, T. S. Pagano, and V. V. Salomonson, "Prelaunch characteristics of the Moderate Resolution Imaging Spectroradiometer (MODIS) on EOS-AM1," *IEEE Trans. Geosci. Remote Sens.*, vol. 36, no. 4, pp. 1088–1100, Jul. 1998.
- [5] X. Xiong *et al.*, "Results and lessons from MODIS reflective solar bands calibration: Pre-launch to on-orbit," *Proc. SPIE*, vol. 6296, p. 629607, Sep. 2006.
- [6] J. Q. Sun, X. Xiong, W. L. Barnes, and B. Guenther, "MODIS reflective solar bands on-orbit lunar calibration," *IEEE Trans. Geosci. Remote Sens.*, vol. 45, no. 7, pp. 2383–2393, Jul. 2007.
- [7] J. Sun, X. Xiong, A. Angal, H. Chen, A. Wu, and X. Geng, "Time-dependent response versus scan angle for MODIS reflective solar bands," *IEEE Trans. Geosci. Remote Sens.*, vol. 52, no. 6, pp. 3159–3174, Jun. 2014.
- [8] D. R. Doelling, D. Morstad, B. R. Scarino, R. Bhatt, and A. Gopalan, "The characterization of deep convective clouds as an invariant calibration target and as a visible calibration technique," *IEEE Trans. Geosci. Remote Sens.*, vol. 51, no. 3, pp. 1147–1159, Mar. 2013, doi: [10.1109/TGRS.2012.2225066](https://doi.org/10.1109/TGRS.2012.2225066).
- [9] R. C. Levy *et al.*, "The Collection 6 MODIS aerosol products over land and ocean," *Atmos. Meas. Techn.*, vol. 6, no. 11, pp. 2989–3034, 2013, doi: [10.5194/amt-6-2989-2013](https://doi.org/10.5194/amt-6-2989-2013).
- [10] A. Lyapustin *et al.*, "Scientific impact of MODIS C5 calibration degradation and C6+ improvements," *Atmos. Meas. Techn.*, vol. 7, no. 12, pp. 4353–4365, 2014.
- [11] P. Minnis *et al.*, "CERES Edition-2 cloud property retrievals using TRMM VIRS and Terra and Aqua MODIS data—Part I: Algorithms," *IEEE Trans. Geosci. Remote Sens.*, vol. 49, no. 11, pp. 4374–4400, Nov. 2011, doi: [10.1109/TGRS.2011.2144601](https://doi.org/10.1109/TGRS.2011.2144601).
- [12] P. Minnis, D. R. Doelling, L. Nguyen, W. F. Miller, and V. Chakrapani, "Assessment of the visible channel calibrations of the VIRS on TRMM and MODIS on Aqua and Terra," *J. Atmos. Ocean. Technol.*, vol. 25, pp. 385–400, Mar. 2008.
- [13] A. Wu, X. Xiong, D. R. Doelling, D. Morstad, A. Angal, and R. Bhatt, "Characterization of Terra and Aqua MODIS VIS, NIR, and SWIR spectral bands' calibration stability," *IEEE Trans. Geosci. Remote Sens.*, vol. 51, no. 7, pp. 4330–4338, Jul. 2013.
- [14] D. Helder, H. Vuppula, L. Ervin, R. Tabassum, and M. Kaewmanee, "PICS normalization: Improved temporal trending using PICS," in *Proc. CALCON*, Aug. 2016.
- [15] H. Chen, X. Xiong, A. Angal, X. Geng, and A. Wu, "Alternative method of on-orbit response-versus-scan-angle characterization for MODIS reflective solar bands," *J. Appl. Remote Sens.*, vol. 10, no. 2, p. 024004, 2016.
- [16] D. R. Doelling *et al.*, "The radiometric stability and scaling of Collection 6 Terra- and Aqua-MODIS VIS, NIR, and SWIR spectral bands," *IEEE Trans. Geosci. Remote Sens.*, vol. 53, no. 8, pp. 4520–4535, Aug. 2015.
- [17] Q. Mu *et al.*, "Assessment of MODIS on-orbit calibration using a deep convective cloud technique," *Proc. SPIE*, vol. 9972, p. 997210, Sep. 2016.
- [18] R. Bhatt *et al.*, "Characterizing response versus scan-angle for MODIS reflective solar bands using deep convective clouds," *J. Appl. Remote Sens.*, vol. 11, no. 1, p. 016014, 2017.
- [19] Q. Mu *et al.*, "Optimization of a deep convective cloud technique in evaluating the long-term radiometric stability of MODIS reflective solar bands," *Remote Sens.*, vol. 9, no. 6, p. 535, 2017.
- [20] X. Geng *et al.*, "Status of time-dependent response versus scan-angle (RVS) for Terra and Aqua MODIS reflective solar bands," *Proc. SPIE*, vol. 9218, p. 92181P, Sep. 2014.
- [21] J.-Q. Sun and X. Xiong, "MODIS polarization-sensitivity analysis," *IEEE Trans. Geosci. Remote Sens.*, vol. 45, no. 9, pp. 2875–2885, Sep. 2007.
- [22] E. J. Kwiatkowska, B. A. Franz, G. Meister, C. R. McClain, and X. Xiong, "Cross calibration of ocean-color bands from Moderate Resolution Imaging Spectroradiometer on Terra platform," *Appl. Opt.*, vol. 47, no. 36, pp. 6796–6810, 2008.
- [23] G. Meister, R. E. Eplee, and B. A. Franz, "Corrections to MODIS Terra calibration and polarization trending derived from ocean color products," *Proc. SPIE*, vol. 9218, p. 92180V, Oct. 2014.
- [24] S. Platnick, J. Y. Li, M. D. King, H. Gerber, and P. V. Hobbs, "A solar reflectance method for retrieving the optical thickness and droplet size of liquid water clouds over snow and ice surfaces," *J. Geophys. Res.*, *Atmos.*, vol. 106, no. D14, pp. 15185–15199, 2001.
- [25] A. Angal, A. Wu, X. Xiong, X. Geng, D. O. Link, and H. Chen, "On-orbit performance of the MODIS SWIR bands," *Proc. SPIE*, vol. 9264, p. 92641Q, Nov. 2014.
- [26] R. E. Murphy, P. Ardanuy, F. J. Deluccia, J. E. Clement, and C. F. Schueler, "The visible infrared imaging radiometer suite," in *Earth Science Satellite Remote Sensing*, vol. 1. New York, NY, USA: Springer-Verlag, 2006, pp. 199–223.
- [27] A. Wu, X. Xiong, and C. Cao, "Tracking on-orbit stability of the response versus scan angle for the S-NPP VIIRS reflective solar bands," *Proc. SPIE*, vol. 9972, p. 99721C, Sep. 2016.

Amit Angal received the M.S. degree in electrical engineering from South Dakota State University, Brookings, SD, USA.

He is currently a Lead Optical Engineer and a Supervisor with Science Systems and Applications, Inc., Lanham, MD, USA, where he is involved in the radiometric characterization and calibration of remote sensing instruments. He is primarily involved in the on-orbit calibration of the reflective solar bands of the Moderate-Resolution Imaging Spectroradiometer (MODIS) instruments on board the terra and aqua spacecraft. He has also supported the CLARREO Mission Preformulation activities in the reflective solar spectrum. In addition, he supports the preflight calibration of the JPSS-2 VIIRS instrument and is involved with the early on-orbit calibration and validation of the JPSS-1 VIIRS instrument. His research interests include cross-calibration between Landsat and MODIS instruments.

Xiaoxiong (Jack) Xiong received the B.S. degree in optical engineering from the Beijing Institute of Technology, Beijing, China, and the Ph.D. degree in physics from the University of Maryland, College Park, MD, USA.

Before joining the NASA Goddard Space Flight Center (GSFC), Greenbelt, MD, USA, he was involved in optical instrumentation, nonlinear optics, laser and atomic spectroscopy, and resonance ionization mass spectrometry at universities, industry, and the National Institute of Standards and Technology. He is currently an Optical Physicist with GSFC, where he is also serving as the Moderate Resolution Imaging Spectroradiometer (MODIS) Project Scientist and the Technical Lead for the MODIS Characterization Support Team and the VIIRS Calibration Support Team.

Qiaozhen Mu received the M.S. degree in geography from Beijing Normal University, Beijing, China, and the Ph.D. degree in climatology from Peking University, Beijing.

She is currently with the Science Systems and Applications, Inc., Lanham, MD, USA, involved in the Moderate Resolution Imaging Spectroradiometer (MODIS) Characterization and Support Team, National Aeronautics and Space Administration, Goddard Space Flight Center, Greenbelt, MD, USA. She is involved in the radiometric calibration and validation of MODIS sensor, and the assessments of calibration performance of satellite Level 1B products.

David R. Doelling received the B.S. degree in meteorology from the University of Utah, Salt Lake City, UT, USA, and the M.S. degree in atmospheric science from the University of Washington, Seattle, WA, USA.

He is currently a Senior Research Scientist with the National Aeronautics and Space Administration Langley Research Center, Hampton, VA, USA, where he is the Time Interpolation and Spatial Averaging Sub-Lead for the Clouds and Earth's Radiant Energy System (CERES) Project and responsible for the diurnal averaging and spatial gridding of CERES footprint cloud and radiative flux parameters. He is also a member of the Geostationary Earth Radiation Budget Experiment, Megha-Tropique, and Absolute Radiance and Refractivity Observatory science teams. He is also the Global Space-Based Inter-Calibration System Visible Calibration Lead.

Rajendra Bhatt received the B.E. degree in electronics engineering from Tribhuvan University, Kirtipur, Nepal, in 2002, and the M.S. degree in electrical engineering from South Dakota State University, Brookings, SD, USA, in 2009.

He is currently a Senior Research Scientist with Science Systems and Applications, Inc., Hampton, VA, USA, in support of on-going radiometric calibration projects at the Climate Science Branch of the NASA Langley Research Center Science Directorate, Hampton, VA, USA. He has played a pivotal role in characterizing and modeling the top-of-atmosphere radiances over multiple invariant Earth targets and utilizing them to uniformly calibrate historical geostationary and AVHRR sensor series to facilitate consistent satellite retrieval products. His research interests include developing techniques of in-flight calibration of geostationary and low-earth orbiting satellite visible observations to assess the sensor's performance on-orbit and ensure the usability of climate data.

Aisheng Wu received the B.S. degree in atmospheric science from the University of Science and Technology of China, Hefei, China, the M.Sc. degree in atmospheric remote sensing from the Chinese Academy of Science, Institute of Plateau Atmospheric Physics, Lanzhou, China, and the Ph.D. degree in bio-meteorology/soil physics from The University of British Columbia, Vancouver, BC, Canada.

He is currently a Senior Scientist with the Moderate Resolution Imaging Spectroradiometer and VIIRS Characterization and Support teams, Goddard Space Flight Center, Greenbelt, MD, USA, and Sigma Space Corporation, Lanham, MD, USA.